Tectonophysics 462 (2008) 164–177

Contents lists available at ScienceDirect

Tectonophysics

journal homepage: www.elsevier.com/locate/tecto

Upper mantle structure of shear-waves velocities and stratification of anisotropy in the Afar Hotspot region

D. Sicilia [a], J.-P. Montagner [a,*], M. Cara [b], E. Stutzmann [a], E. Debayle [b], J.-C. Lépine [a], J.-J. Lévêque [b], E. Beucler [c], A. Sebai [a], G. Roult [a], A. Ayele [d], J.M. Sholan [e]

[a] Laboratoire de Sismologie, CNRS- UMR7154, Institut de Physique du Globe, Université Paris 7-Diderot, 4 place, Jussieu, F-75252 Paris Cedex 05, France
[b] CNRS-EOST, Université Louis Pasteur, 5 rue Descartes, Strasbourg F-67084, France
[c] Laboratoire de Planétologie et Géodynamique, Université de Nantes, BP92205, 2 rue de la Houssinière, 44322, Nantes, France
[d] Geophysical Observatory, University of Addis Ababa, Ethiopia
[e] National Seismological Observatory Center, Dhamar, Republic of Yemen

ARTICLE INFO

Article history:
Received 18 January 2007
Received in revised form 25 February 2008
Accepted 25 February 2008
Available online 26 August 2008

Keywords:
Afar Hotspot
Seismic tomography
Surface waves
Anisotropy
Stratification

ABSTRACT

The Afar area is one of the biggest continental hotspots active since about 30 Ma. It may be the surface expression of a mantle "plume" related to the African Superswell. Central Africa is also characterized by extensive intraplate volcanism. Around the same time (30 Ma), volcanic activity re-started in several regions of the African plate and hotspots such as Darfur, Tibesti, Hoggar and Mount Cameroon, characterized by a significant though modest volcanic production. The interactions of mantle upwelling with asthenosphere, lithosphere and crust remain unclear and seismic anisotropy might help in investigating these complex interactions.

We used data from the global seismological permanent FDSN networks (GEOSCOPE, IRIS, MedNet, GEO- FON, etc.), from the temporary PASSCAL experiments in Tanzania and Saudi Arabia and a French deployment of 5 portable broadband stations surrounding the Afar Hotspot. A classical two-step tomographic inversion from surface waves performed in the Horn of Africa with selected Rayleigh wave and Love wave seismograms leads to a 3D-model of both S_V velocities and azimuthal anisotropy, as well as radial S_H/S_V anisotropy, with a lateral resolution of 500 km. The region is characterized by low shear-wave velocities beneath the Afar Hotspot, the Red Sea, the Gulf of Aden and East of the Tanzania Craton to 400 km depth. High velocities are present in the Eastern Arabia and the Tanzania Craton. The results of this study enable us to rule out a possible feeding of the Central Africa hotspots from the "Afar plume" above 150–200 km. The azimuthal anisotropy displays a complex pattern near the Afar Hotspot. Radial anisotropy, although poorly resolved laterally, exhibits S_H slower than S_V waves down to about 150 km depth, and a reverse pattern below. Both azimuthal and radial anisotropies show a stratification of anisotropy at depth, corresponding to different physical processes. These results suggest that the Afar hotspot has a different and deeper origin than the other African hotspots (Darfur, Tibesti, Hoggar). These latter hotspots can be traced down to 200 km from S-wave velocity but have no visible effect on radial and azimuthal anisotropy.

1. Introduction

Hotspots are geological objects which cannot be explained by plate tectonics. They probably play an important geodynamic role in the continental breakup and are often associated with catastrophic events, such as the trapp episodes (Courtillot et al., 1999). Many hotspots are supposed to be the surface expression of a deep mantle plume (Morgan, 1971; Montelli et al., 2004), but one major difficulty is still the determination of their depth of origin, since their lateral extension at depth is thought to be small (<200 km), making their seismic detection problematic.

Plumes could come from any of the thermal boundary layers of the mantle. As summarized by Courtillot et al. (2003), 3 families of hotspots and plumes can be discriminated and might originate from the Core-Mantle Boundary (CMB), the transition zone or the boundary between the lithosphere and the asthenosphere. Although the very deep plume origin is favoured by a large part of Earth scientists, some of them do not believe that seismic anomalies detected at depth in the upper mantle beneath hotspots, would be connected with a lower mantle rising material. For example, Foulger et al. (2001) do not believe in the hotspot hypothesis below Iceland and Anderson (2000, 2001) preferred to associate plume-like upwellings with small-scale,

* Corresponding author. Tel.: +33 1 44 27 48 95; fax: +33 1 44 27 38 94.
E-mail address: jpm@ipgp.jussieu.fr (J.-P. Montagner).

0040-1951/$ – see front matter © 2008 Elsevier B.V. All rights reserved.
doi:10.1016/j.tecto.2008.02.016

edge-driven convection (King and Ritsema, 2000) in the upper mantle (probably with an asthenospheric origin). A better understanding of the interaction between upwelling, asthenosphere and lithosphere might help to discriminate competing models.

The Afar Hotspot, located in the continental environment of the Horn of Africa, is one of the most active hotspots in the world (e.g. Courtillot et al., 2003). The tectonic event that still affects the region can be dated back 30 Ma ago, when Africa and Arabia formed a single continent. In the Oligocene (≈28 Ma), a period of intense magmatism uplift (Mohr, 1983; Courtillot et al., 1999) started and produced a crustal bulge with some fractures (Barberi et al., 1975) due to the weakening of the lithosphere and a large flood basalt province. The high flood basalt plateaus in Yemen and Ethiopia are the signature of these voluminous eruptions. Then, the first important phase of E–W extension occurred before a second phase of N–S extension (Jestin and Huchon, 1992) and created the rifts of Red Sea and the Aden Gulf, covered by water in the Miocene (15 Ma). These two rifts have not merged yet, but they are connected through the Afar Depression. Central Africa is also characterized by extensive intraplate volcanism. Around the same time (30 Ma), volcanic activity re-started in several regions of the African plate and hotspots such as Darfur, Tibesti, Hoggar and Mount Cameroon (Fig. 1) , were characterized by a significant though modest volcanic production during the Cenozoic and Quaternary (Burke and Wilson, 1976; Wilson and Guiraud, 1992).

From a seismological point of view, several tomographic regional studies with a lateral resolution of 1000 km and over for plate-scale studies down to approximately 100 km for local studies, were conducted on the African continent and Saudi Arabia (Hadiouche et al., 1989; Knox et al., 1998; Ritsema and van Heijst, 2000; Debayle et al., 2001; Sebai et al., 2006; Benoit et al., 2006; Hansen et al., 2006). All these authors find low velocities beneath Afar and western Saudi Arabia down to at least 250 km. Knox et al. (1998) estimate the difference to be 0.2–0.8 km/s lower than PREM at 100 km depth from Rayleigh wave dispersion of fundamental mode. With the addition of higher mode data, Debayle et al. (2001) found a slow anomaly down to the upper/lower mantle boundary. Ritsema et al. (1998) inverted a global dataset of fundamental and higher mode surface waves together with long period body waves that sample the lower mantle. They found a slow shear-wave velocity anomaly in the lower mantle beneath Southern Africa. This negative anomaly, tilted by 45° might be associated with upwelling materials reaching the upper mantle in the Horn of Africa (Ritsema et al., 1999). On the other hand, by using receiver functions Nyblade et al. (2000) estimate a transition zone thickness similar to the global average thickness, and suggest a shallower origin for a possible plume beneath the region. The P-wave tomographic model of Benoit et al. (2006) reveals beneath Ethiopia an elongated and wide low wave speed anomaly down to at least 400 km depth. All these results are consistent with a thermal anomaly beneath the region although its origin at depth and geometry is still debated. Both a single broad plume or several narrow conduits could create the large velocity contrast observed in the upper mantle (Debayle et al., 2001). More recently, Montelli et al. (2004) claimed a very deep origin of the Afar hotspot. The detection of the tail of Afar upwelling in the lower mantle is beyond the scope of the paper since our fundamental mode surface wave dataset restrict the sensitivity to the uppermost 400 km of the mantle.

However, the issues of similarities or differences between Afar hotspot and other African hotspots, as well as their possible connection is still debatable. Hadiouche et al. (1989) by use of a vectorial tomography technique (Montagner and Jobert, 1988), which enables to simultaneously retrieve S-wave velocity and anisotropy, suggested that the Afar plume might feed below lithosphere other hotspots in central Africa. Ebinger and Sleep (1998) came to the same conclusion by using geological and gravity data. We will focus on the characterization of the plume–lithosphere interaction and its connection with other African hotspots in the uppermost mantle beneath the Eastern part of the African continent. In order to address these issues, a temporary experiment in the Horn of Africa and Southern Arabia was carried out. A companion paper (Sebai et al., 2006) used a very similar dataset and techniques but was devoted to the tomography of the whole African continent, and its lateral resolution of anisotropy was limited to 1000 km. Thanks to a temporary regional-scale

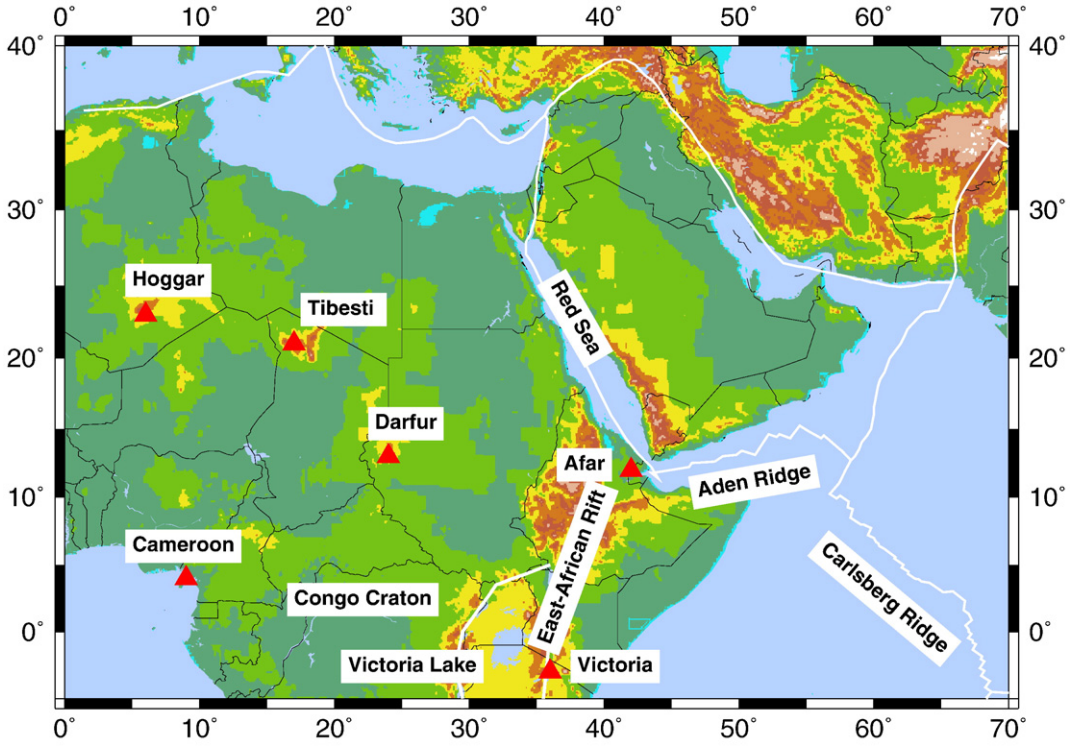

Fig. 1. Geographic map of the North and East of Africa with the most important geological features. The red triangles represent the hotspots.

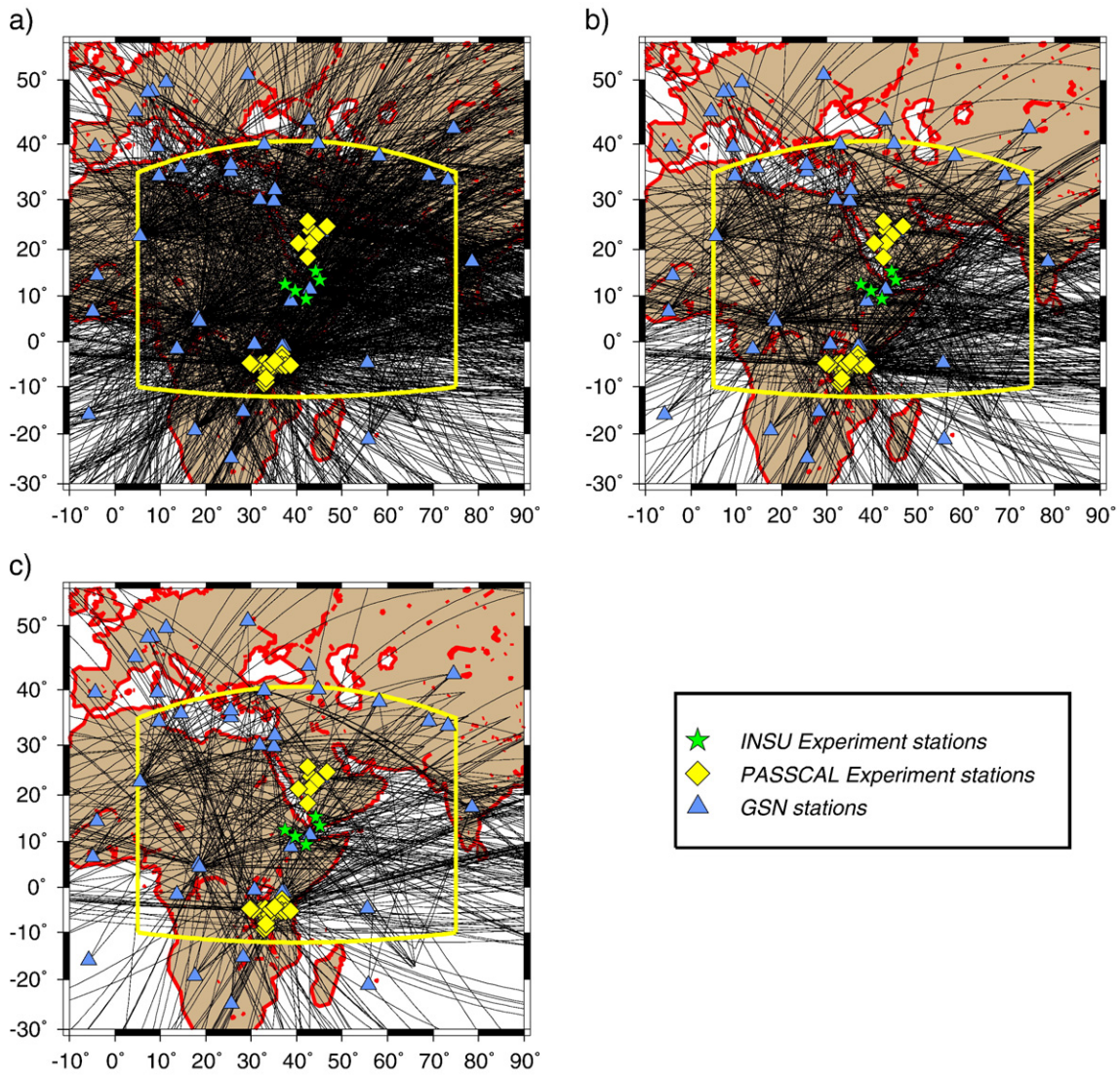

Fig. 2. Geographical distribution of the 1764 Rayleigh (a) and 744 Love (b) paths used in the inversion with stations location. (c) Geographical distribution of the 430 paths common to the Rayleigh and Love waves. Permanent stations from the GEOSCOPE, IRIS, GEO-FON and MedNet networks are represented by triangles. Temporary broad-band stations from the PASSCAL experiments are shown with diamonds and those from the INSU experiment with stars. The inversion is performed within the yellow box.

network surrounding the Afar hotspot, the densification of paths in Eastern Africa enables to derive a 3D tomographic model of S-wave velocity and anisotropies with an enhanced lateral resolution of 500 km. If LPO (lattice preferred orientation) of olivine (Nicolas and Christensen, 1987) is assumed to be the dominant mechanism of deformation in the upper mantle, the mapping of anisotropy (radial and azimuthal) should enable to investigate how mantle flow is perturbed by the existence of several upwellings beneath Central and Eastern Africa.

2. Data selection

The station coverage of the African continent by permanent broadband seismic stations is still poor. However, for deriving a tomographic study of velocity and anisotropy, it is necessary to have a very good spatial coverage of the region under investigation as well as an azimuthal distribution as good as possible. The permanent stations belong to the FDSN networks (GEOSCOPE, IRIS, MedNet, GEOFON, etc.). To complement the poor broadband station coverage of the Horn of Africa area, a temporary experiment was designed. Five more broadband stations equipped with STS-2 seismometers provided by the INSU (National Institute of Universe Sciences) network RLBM (broadband portable network) were deployed in Ethiopia and Yemen in the vicinity of the Afar triangle (Fig. 2 and Table 1), in the framework of the French program "Horn of Africa" which started in summer 1999 and ended in 2002. Additional data from the PASSCAL experiments in Tanzania and Saudi Arabia provided by the IRIS DMC were also used. All events with a magnitude larger than 5.7 and a good signal-to-noise ratio were selected for this study. We used the Harvard centroid moment tensor (CMT) to calculate synthetic seismograms. In order to meet the requirements of the method (see Section 3), only events with

Table 1
Temporary INSU stations coordinates

Station	Latitude [°]	Longitude [°]	Elevation [m]
Alemaya (ALE)	9.42	42.02	1551
Dessie (DSS)	11.12	39.63	2538
Gondar (GDR)	12.58	37.45	2134
Sanaa (SAY)	15.21	44.11	2265
Yafe (YAF)	13.87	45.23	2307

epicentral distances between 30° and 135° were kept, thus avoiding that the fundamental mode would overlap with higher modes signal.

After visual inspection of more than 40,000 seismograms and strict selection procedure, 1764 paths for the Rayleigh waves and 744 for the Love waves were selected. Since many paths originated from the same seismogenic zones (primarily the Pacific rim) and do not improve the azimuthal coverage, we only kept the seismograms with the best signal-to-noise ratio. The geographical distribution of the Rayleigh and Love paths is plotted in Fig. 2. The regionalisation algorithm Montagner (1986) allows us to compute the final model in an area smaller than the region covered by the paths. Although the inversion is performed over the global Earth, the spatial and azimuthal coverages are optimal for the regional investigation around the Afar hotspot in Eastern Africa. Therefore, only the results within the box of latitude −10°S to 35°N and longitude 5°E to 60°E are presented here.

3. Phase velocity measurements

The phase velocity of the fundamental mode of surface waves along each great circle path is determined by using the inverse method developed by Beucler et al. (2003) named the "roller coaster" waveform inversion technique for surface waves. The roller coaster technique was designed to simultaneously retrieve the fundamental and higher mode phase velocities of surface waves. We use it for only retrieving the fundamental mode phase velocity. This technique enables to deal with the non-linearity of the inverse problem associated with the retrieval of phase velocity from seismic wavetrains. It first detects all possible solutions in a broad frequency range. In a second stage, starting from each of these solutions, it finds around a given frequency, the best phase velocity. A least-squares optimization is used in order to match small variations in the model space of phase velocities. So the calculation of the phase velocity is a two-step procedure, in the sense that all possible models of phase velocity in the 4–25 mHz frequency range are first detected. It is assumed that the reference model (PREM) fits the data well at long periods (>200 s). The exploration of the parameter space (phase velocities along a path) is done by steps of 0.1% between −5% and +5% of the PREM values. All minima in the oscillatory misfit function are considered as candidates for starting the second step using a linear least-squares inversion (Tarantola and Valette, 1982) in order to refine the model. Minimizing the misfit function of each computation (difference between data and seismograms) will then give the final value of phase velocity. The roller-coaster technique enables the analyst to reliably retrieve the average phase velocity cR(T) along the path between the source *S* and the receiver *R*.

Both recorded signals and synthetics are bandpass-filtered between 40 and 500 s and a time window is applied to extract the fundamental modes of Love and Rayleigh waves. Synthetic seismograms are calculated by normal mode summation as described in Woodhouse and Girnius (1982).The different time windows are computed using synthetic mode-branch wave trains and are checked manually. The signals that cannot be accurately detected are rejected. At this stage, 3216 among 41505 seismograms have been kept for the 3 components. Many seismograms were rejected because the associated paths do not provide additional information. For example, many earthquakes occurred in the Western Pacific at clustered locations. The purpose is optimize azimuthal coverage across Eastern Africa. To illustrate the selection procedure, we show in Fig. 3 the vertical

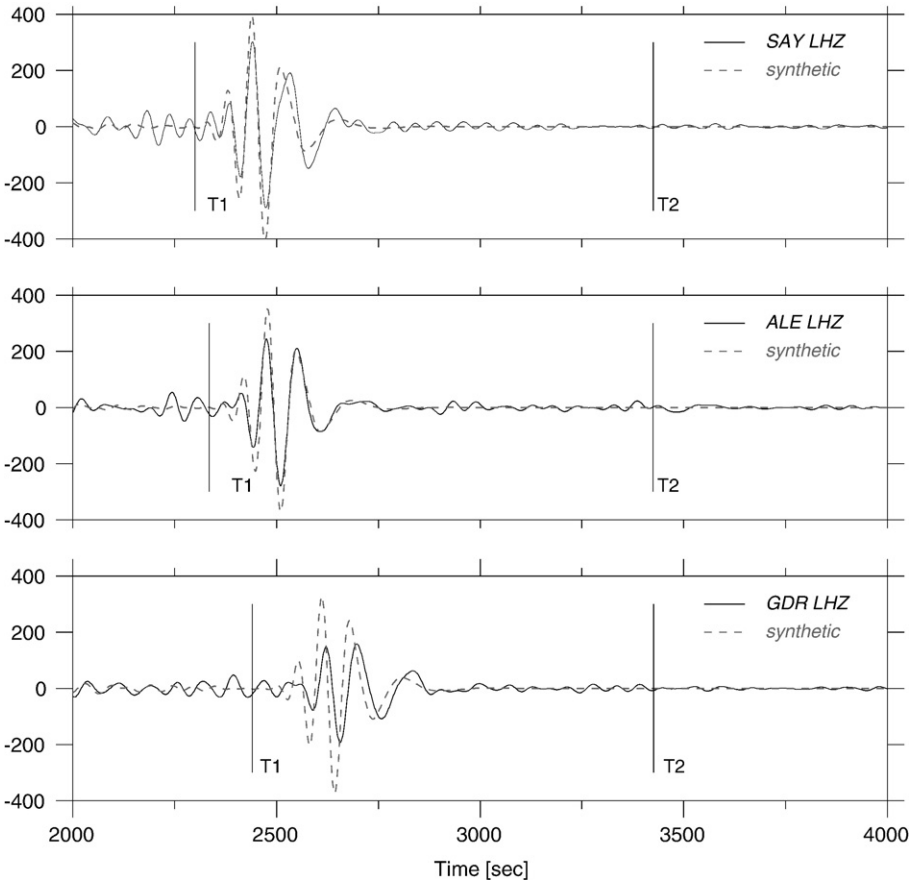

Fig. 3. The vertical component of the real data of the stations SAY, ALE and GDR (solid line) and the corresponding synthetic seismograms (dotted line) computed in the PREM model. The fundamental mode of the real and synthetic data are picked between the time window (T1–T2). This earthquake occurred on May 14, 2000 at 4.31S, and 123.56E with a magnitude of 5.9. The respective epicentral distances are 9043 km, 9200 km and 9700 km.

components of three of the five temporary stations (ALE, SAY and GDR) for the May 14, 2000 Sumatra earthquake. The waveforms of synthetic seismograms of SAY and ALE stations are similar to the recorded seismograms but a large time shift can be noted between real and synthetic signals at the GDR station. The synthetic Rayleigh waves arrive before the real data and this latter signal has a smaller amplitude. The meaning of this delay will be explained in Section 5. After picking time windows, the inversion is performed only at frequencies with large enough amplitudes, above a threshold fixed to 10% of the mean maximum spectra amplitude. The inverse problem is expressed in terms of phase velocity perturbations along the path between the source *S* and the receiver *R*, as explained in Beucler et al. (2003) by the roller-coaster technique. An example is given in Fig. 4, where the phase velocities corresponding to the data represented in Fig. 3 are plotted with their error bars. It can be noted that the computed phase velocities at stations SAY and ALE are relatively close to the *a priori* velocities. On the contrary, the phase velocities obtained at GDR station are slower than those of PREM values. The phase velocity uncertainties are estimated by computing the a posteriori covariance matrix of parameters (phase velocities) and by taking the square root of the diagonal elements. Another way to check the inversion reliability is to measure, in the time domain, the waveform differences between the shifted synthetic seismogram and the data. Each reconstructed seismogram is then qualitatively compared with the data (Fig. 5).

4. The tomographic procedure

4.1. Methodology

In order to obtain a 3-D image of the upper mantle beneath the Horn of Africa, we follow a classical two-step procedure used in previous studies (Hadiouche et al., 1989; Montagner and Tanimoto, 1991; Stutzmann and Montagner, 1994; Debayle and Lévêque, 1997; Griot et al., 1998; Debayle et al., 2001, 2005; Sebai et al., 2006). First, the method consists in regionalizing the average phase velocities CR (T) computed in Section 3, in order to retrieve the local phase velocity C(T,M) at each point M(θ,φ) along the path and at different periods T. For this purpose, we use the continuous regionalization algorithm of Montagner (1986). It is assumed that the geometrical optics approximation is valid for surface waves. The 2-step procedure is reversed in Debayle and Lévêque (1997), Debayle et al. (2001), where the first step is the inversion at depth of VS(z) and the second step the regionalization.

It is a strong hypothesis since only large scale heterogeneities can be retrieved. To go beyond the ray theory, it is necessary to take

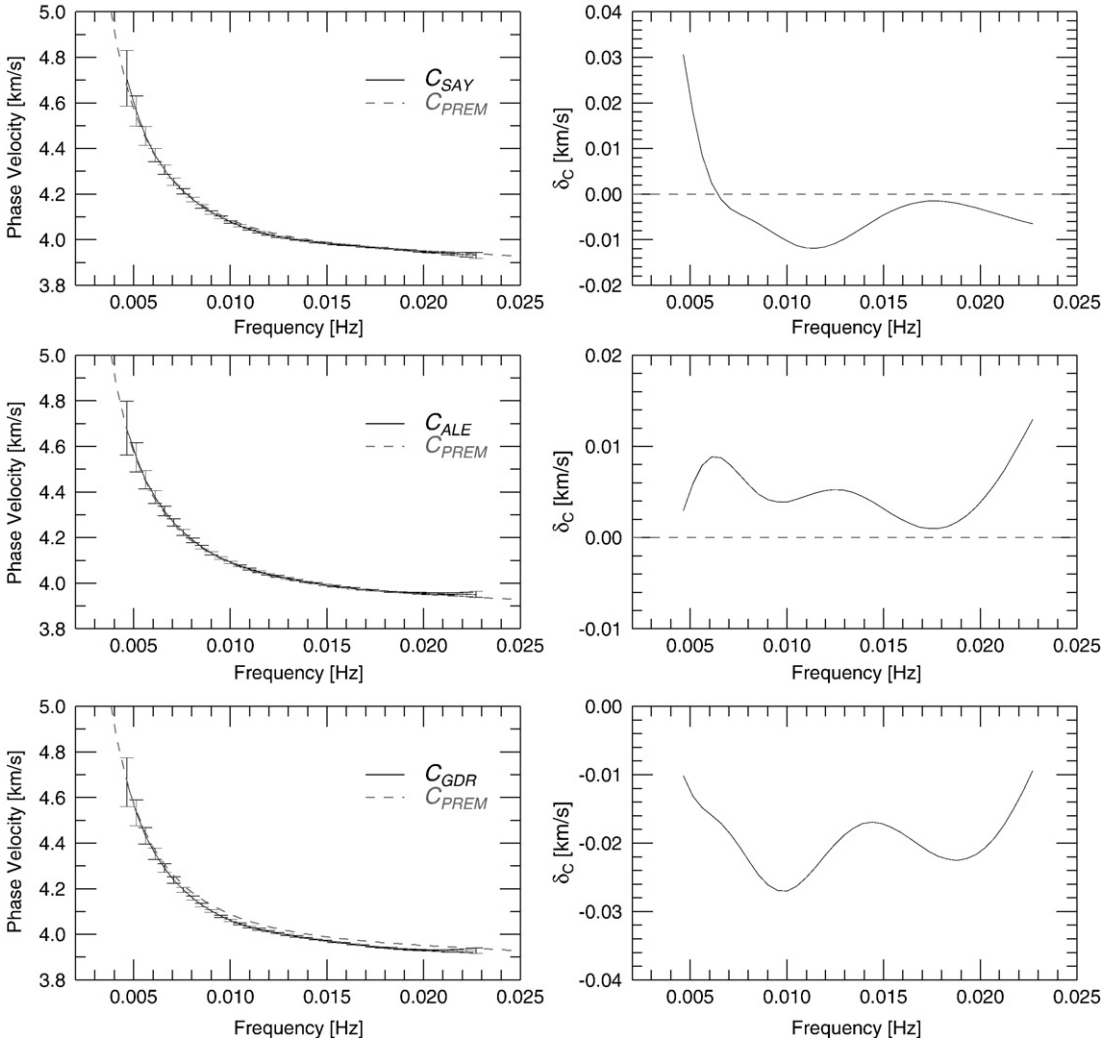

Fig. 4. (Left) Phase velocities measured (solid line) for the stations SAY, ALE and GDR and the corresponding error bars for the same earthquake. The phase velocity of the PREM is plotted with a dotted line. The frequency range is between 2 mHz and 25 mHz (respectively 500 s and 40 s). (Right) δC represents the difference between the data phase velocity and the synthetic one.

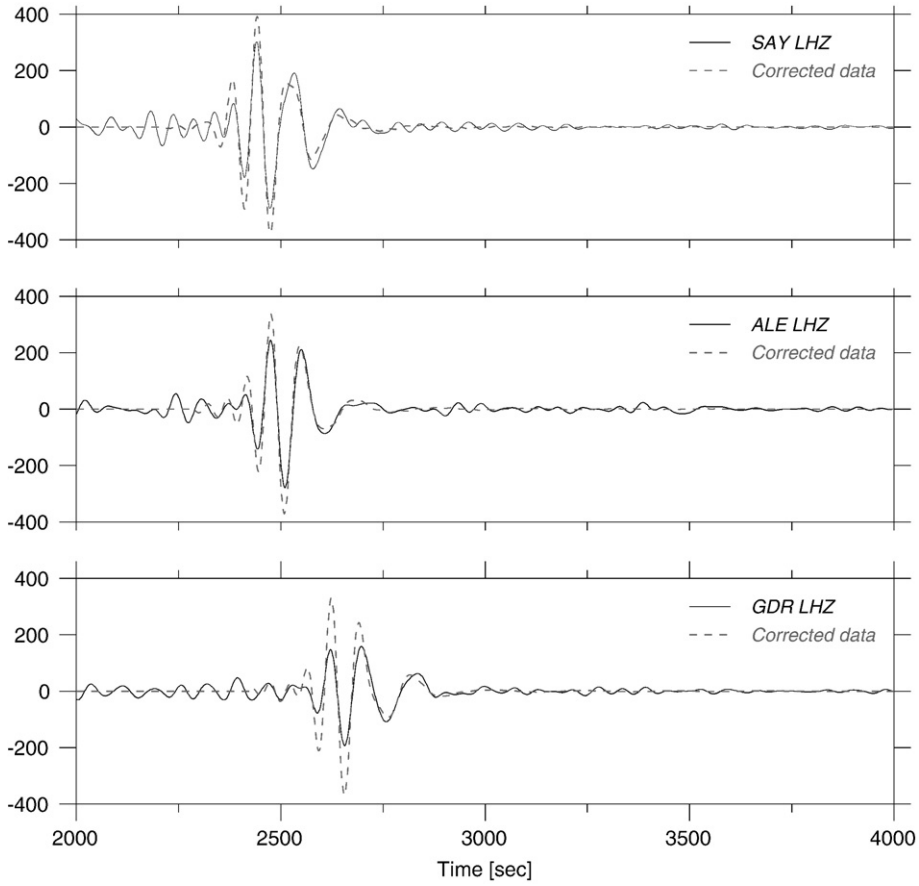

Fig. 5. Comparison between the real data before inversion (solid line) and the synthetic modified with the inversion results obtained in Fig. 4 (dotted line). It can be observed that the phase velocities of the fundamental modes are retrieved well.

account of the finite-frequency effect when length scale has the same order of magnitude as the seismic wavelength. For a point scatterer, the kernel displays a typical shape of banana-doughnut (Dahlen et al., 2000). However, several studies showed that ray theory surface wave tomography with a very dense path coverage, can detect heterogeneities with length scales close and even smaller than the seismic wavelength. In addition, since our tomographic technique (Montagner, 1986) convolves the ray path with a Gaussian covariance function with a correlation length of 500 km (in this study), it approximately takes account of sensitivity of surface waves to zones around the ray. The average phase velocity is linearly related to the local phase velocity as follows (Sato and Santo, 1969):

$$\frac{\Delta}{C_R(T)} = \int_S^R \frac{1}{C(T,M)} ds \tag{1}$$

where Δ is the epicentral distance between source S and receiver R. The advantage of the inversion technique of Montagner (1986) is the simultaneous calculation of the local phase velocity and azimuthal anisotropy anomalies. Using Rayleigh's principle, Smith and Dahlen (1973) have shown that in a slightly anisotropic Earth, the local phase velocity at a given point M depends on the path azimuth ψ:

$$C(T,M) = C_0(T,M)\Big[1 + \alpha_0(T,M) + \alpha_1(T,M)\cos 2\psi(M) + \alpha_2(T,M)\sin 2\psi(M) + \alpha_3(T,M)\cos 4\psi(M) + \alpha_4(T,M)\sin 4\psi(M)\Big] \tag{2}$$

where α_0 corresponds to the "isotropic" velocity (averaged over all azimuths) later on referred to as the 0Ψ term, α_1, α_2 (2Ψ terms), α_3 and α_4 (4Ψ terms) are the coefficients of azimuthal anisotropy, and C_0 is the isotropic velocity of the reference model. Montagner and Nataf (1986) showed that Rayleigh waves are mainly sensitive to 2ψ coefficients and Love waves to 4ψ coefficients. Therefore, we have neglected the terms in 4ψ for the inversion of Rayleigh waves, and those in 2ψ for Love waves. All the inverted terms are filtered by a correlation length L (Montagner, 1986). The choice of L is primarily conditioned by the spatial coverage of paths in the area under investigation. The α_i terms can then be inverted at depth by using a set of partial derivatives proportional to the partial derivatives of a transversely isotropic medium with a vertical axis of symmetry (Montagner and Nataf, 1986). This constitutes the second step of the tomographic procedure which is explicitly described in Montagner and Jobert (1981). The different azimuthal terms depend on several combinations of the elastic coefficients, but the surface wave information is not sufficient to correctly resolve all the parameters (Nishimura and Forsyth, 1989). Therefore, though all parameters are inverted for, only results of the most reliable parameters (Montagner and Tanimoto, 1991) will be presented in the next section: the shear-wave velocity V_{SV}, the amplitude of S_V-azimuthal anisotropy G with the azimuth of the fast axis direction ψ_G and the radial anisotropy described by the parameter $\xi=(V_{SH}/V_{SV})^2$. This second kind of anisotropy expresses the relative importance of the azimuthal averages of the transverse horizontally polarized S-wave of velocity (V_{SH}) and vertically polarized S-wave of velocity (V_{SV}) for a horizontal wave vector. The ξ parameter is obtained by the simultaneous inversion of the 0Ψ terms of Rayleigh and Love waves (α_0(T,M) in Eq. (2). While the G azimuthal anisotropy provides information about the direction of horizontal material flow, the classical interpretation of ξ in terms of olivine LPO (lattice preferred orientation) provides

information about the orientation of the material flow in the vertical plane. When $\xi>1$, the flow can be interpreted as horizontal or subhorizontal whereas the case $\xi<1$ corresponds to a vertical or subvertical flow (see for example Montagner, 1994).

4.2. Results

Lateral perturbations of S_V -wave velocities and the S_V-azimuthal anisotropy (G-parameter) are presented in Fig. 6a and b. These results

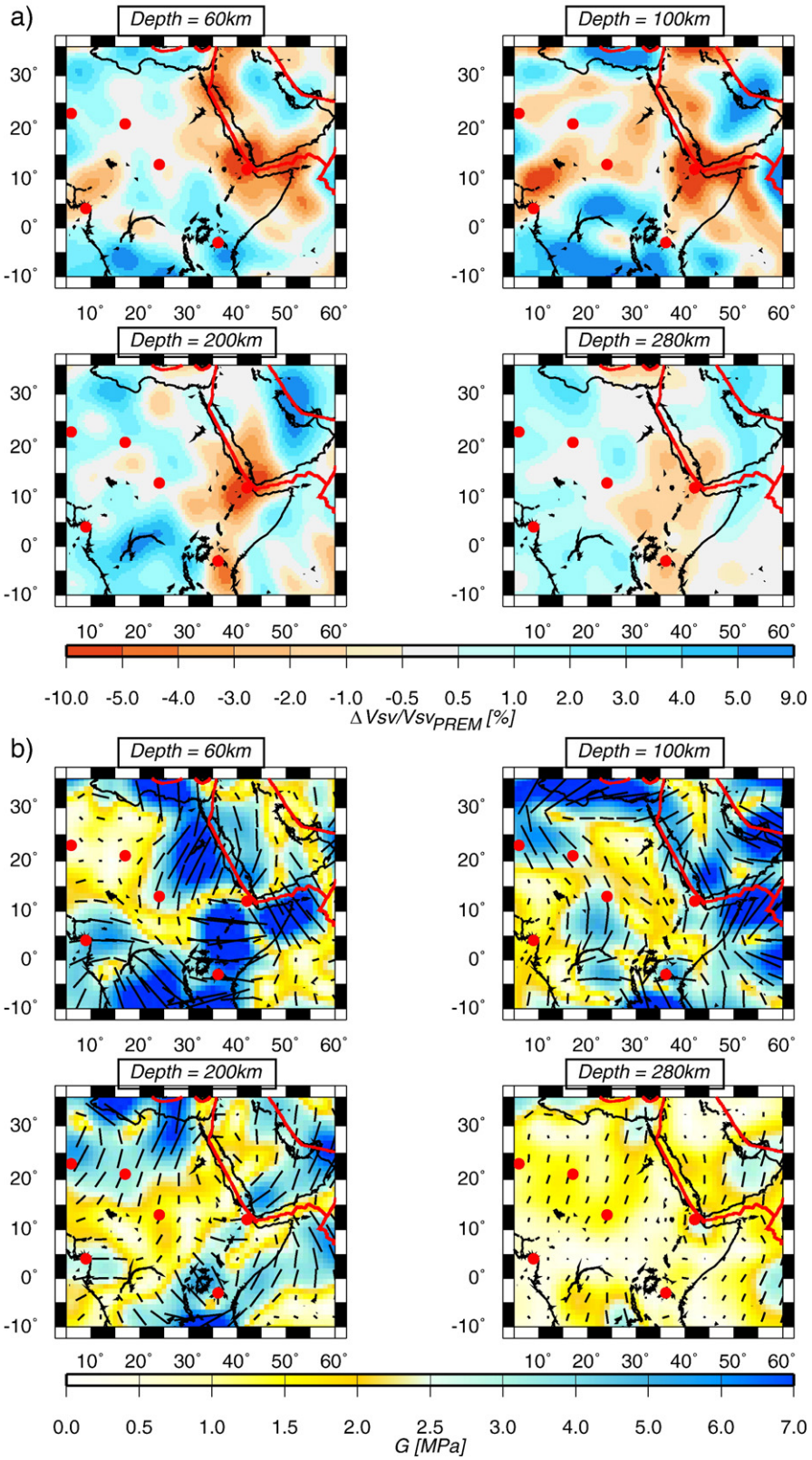

Fig. 6. (a) Perturbations of the S_V-wave velocities expressed relative to the PREM values at 60 km (top left), 100 km (top right), 200 km (bottom left) and 280 km (bottom right) depth. (b) The azimuthal anisotropy (G parameters) with the fast directions of horizontally propagating S_V-waves. The red circles correspond to the African hotspots in the list of Courtillot et al. (2003).

are displayed for three depths, 60 km, 100 km, 200 km and 280 km. These parameters, as explained in the previous section, D can be interpreted in terms of convective flow and then provide information on mantle geodynamics.

At all depths, the largest slow anomaly is located below the Afar Hotspot, at the intersection of the three divergent rifts: the Red Sea, the Gulf of Aden ridge and the East-African Rift. At 60 km and 100 km depth, a large zone of very slow velocities surrounds the hotspot and extends along the Red Sea, the Gulf of Aden and up to Northern Arabia. Other hotspots like Tibesti, Darfur, Cameroon, Victoria (Fig. 1) fall onto the boundary between fast and slow velocity anomalies. On the other hand, fast wave velocities are observed beneath the Tanzania Craton and the Eastern part of Southern Arabia as expected for old cratons. The Congo Basin, a late Proterozoic to Cenozoic structure (Daly et al., 1992) also shows fast velocities. The Carlsberg Ridge presents fast velocities between 5° and 15°N, but the same observation can be made on most of global phase velocity maps (Ekström et al., 1997; Grand et al., 1997) and regional tomographic studies (Debayle and Lévêque, 1997; Debayle et al., 2001).

At 200 km depth, the signature of the Afar Hotspot is less pronounced but still prominent. A broad N–S zone from Southern Egypt to Southern Ethiopian Rift down to Victoria hotspot is the dominant structure of slow velocities. These maps at different depths are very similar to those obtained by Ritsema and van Heijst (2000) and Sebai et al. (2006) in a large-scale regional study of the Africa continent.

Our model shows a very localized slow anomaly beneath the Afar Hotspot in the whole depth range, whereas the model of Debayle et al. (2001) displays a more diffuse anomaly, extending to Red Sea, Gulf of Aden and Saudi Arabia. The results presented here show slightly faster velocities beneath the Nubian Craton, West of Red Sea than in the model of Debayle et al. (2001) at 100 km depth. Both models show a sharp transition from low to high velocities respectively in Southern Ethiopian Rift and the Tanzania Craton. The comparison cannot be done West of 20°E, due to a weak resolution induced by a poor path coverage in the model of Debayle et al. (2001).

The anisotropy patterns (Fig. 6b) show the directions of the fastest propagating waves and the corresponding amplitude. As the depth increases, the amplitude of azimuthal anisotropy decreases and to first order, the directions of the fast axis become oriented south-north at large depths, in most parts of the African plate north of equator, except around Afar. We also observe an almost south-north direction along the Aden Ridge. At shallow depths (60, 100 km), we see a complex distribution of anisotropy with a very perturbed pattern around the Afar Hotspot. The azimuthal anisotropy directions in Arabia agree with the shear-wave splitting studies. Wolfe et al. (1999) and Hansen et al. (2006) find from temporary experiments, N–S directions in Western Saudi Arabia, similar to that recovered in our models. Barruol and Ismail (2001) analyzed SKS-wave measurements at GEOSCOPE and IRIS stations. Except at ATD (11.53N/42.85E) in Djibouti, the polarization directions are very similar. In agreement with Gao et al. (1997) from a temporary experiment at eastern Victoria Lake and Barruol and Ismail (2001) at the KMBO station, we found fast axis directions oriented subparallel to the Ethiopian Rift at 100 km depth but orthogonal to the rift at 200 km depth. Either preferred alignment of melt-filled pockets, with a long axis oriented parallel to the maximum compressive direction and a short axis oriented parallel to the extension direction (Kendall et al., 2005), or preferred alignment of olivine *a*-axis parallel to the trend of the rift may explain these observations (Barruol and Ismail, 2001; Gao et al., 1997). At larger depth (280 km), the azimuthal anisotropy is very small, but it primarily displays a south-north orientation in most Eastern Africa.

The simultaneous inversion of the 0Ψ-terms of Rayleigh and Love waves phase velocities also enables us to retrieve the radial anisotropy, represented by the ξ parameter. However, as can be seen on Fig. 2, the distribution of Rayleigh paths is much better than the path coverage of Love waves. Consequently, we do not show the 4Ψ-Love wave azimuthal anisotropy. But we invert the 4Ψ term to avoid possible bias of the 0Ψ-term by this kind of azimuthal anisotropy (the average over all azimuths can be different from zero in case of poor azimuthal coverage). The maps of radial anisotropy deviations with respect to PREM at 60 km, 100 km, 200 km and 280 km are plotted in Fig. 7 and can be compared with the perturbations of the S_V-wave velocities (Fig. 6a).

At 60 km and 100 km depth, the $\delta\xi(=\xi-\xi_{PREM})$ parameter is overall positive, except below the Ethiopian rift, the Red Sea and the Aden Ridges where it is strongly negative. This has commonly been associated with vertical material flow. At 200 km depth, the overall amplitude of radial anisotropy is weaker and the most negative values of the ξ parameter are observed along the Red Sea and beneath the east African rift, suggesting upgoing mantle material here. Surprisingly the radial anisotropy is strongly positive below the Afar hotspot and the strongest spot of negative $\delta\xi$ has moved south-west of Afar. At depth larger than 250 km (Fig. 7), the amplitude of $\delta\xi$ is rather small except the strong positive anomaly below the Afar hotspot and negative spot around 3°N.

We note that the perturbations of ξ reach extreme positive values at 100 km depth. Debayle and Kennett (2000) also found similar strong radial anisotropy at lithospheric depths in Australia and note that it is difficult to reconcile these extreme values with current mineralogical models. They suggest that the presence of strong lateral heterogeneities along the paths or effects introduced by the assumption of transverse isotropy in their starting PREM model might explain these extremely high ξ values. In our model, the influence of Love wave higher modes on the phase velocity measurements of the fundamental mode might be also invoked as a possible explanation for these high ξ values, since overtones arrive nearly at the same time as the fundamental mode and their isolation by applying a simple time window is sometimes difficult. To check this point, we have performed a synthetic test (see Appendix 2) which demonstrates that higher modes do not induce any problem. Because the events collected in this study do not have an origin deeper than 200 km, the higher modes are therefore not sufficiently excited. It is found that the fundamental mode phase velocity measurements are not significantly affected by our procedure.

5. Discussion and conclusion

From a broad-scale gravimetric study, Nyblade (1994) suggests that the upper mantle beneath the Eastern part of Africa reflects the signature of a deep super-plume located in the lower mantle beneath the southeastern Atlantic Ocean. At global scale, Ritsema et al. (1999) combined long period body waves with fundamental and higher mode surface waves to achieve a good resolution in the whole mantle. They propose that Eastern Africa is fed through a tilted low velocity anomaly rising from the core-mantle boundary (CMB) beneath the Southeastern Atlantic Ocean. At regional scale, Debayle et al. (2001) observe slow S_V-waves in the upper mantle transition region beneath the Horn of Africa from the inversion of fundamental and higher mode Rayleigh waves. Their model does not have any resolution in the lower mantle but suggests that the deep anomaly extending from the CMB in global tomography might provide the source for upwelling material responsible for the slow anomaly that they observe in the transition zone beneath Southwest Arabia. But Benoit et al. (2006) find that the center of slow anomaly shifts to the west with depth. These models can be made compatible with the results of laboratory experiments of Davaille (1999) as illustrated by Courtillot et al. (2003) which suggest that thin conduits associated with hotspots originate from a large dome in the lower mantle, but the seismic detection of thin conduits in the

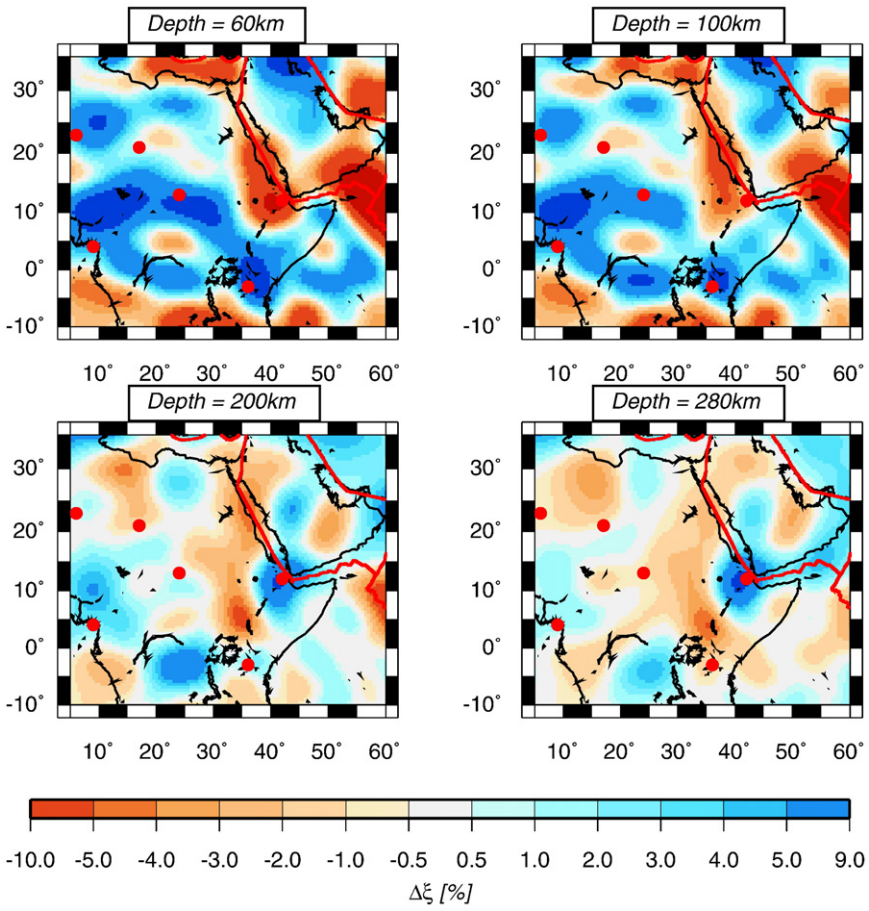

Fig. 7. Values of the parameter ξ which defines the radial anisotropy $(V_{SH}/V_{SV})^2$, at the same depths as Fig. 6, with respect to PREM (Dziewonski and Anderson, 1981). The red circles correspond to the African hotspots in the list of Courtillot et al. (2003).

deep upper and lower mantles is problematic. Our study cannot find the deep origin at depth of upwellings, but we can investigate the interaction of upwellings with asthenosphere and lithosphere and rule out some hypotheses about them.

The tomographic procedure of this study makes use of a robust technique of phase velocity measurements (Beucler et al., 2003) and enables us to retrieve simultaneously the shear-wave velocity and the anisotropy perturbations in the upper mantle beneath the Horn of Africa. Part of the dataset was used in Sebai et al. (2006) for a tomographic investigation of the whole African plate. The contribution of temporary stations in addition to permanent stations is fundamental since this additional dataset allows our 3D S_V-wave and anisotropy model to be constrained with a lateral resolution of around 500 km in the region under study. With the present dataset, it is possible to address the issue of the interaction between mantle upwellings with asthenosphere and lithosphere below eastern Africa around the Afar hotspot.

5.1. East–West North–South asymmetry of structures

Depth cross-sections showing distributions of the different parameters are plotted on Fig. 8, where the shear-wave velocities, the amplitude of the parameter *G* and the parameter δξ are displayed on two vertical cross-sections. One profile (W1-E2) has an almost East–West orientation and crosses the Afar Hotspot and the Darfur (Jebel Mara) as well as the Tibesti and Hoggar hotspots. The other profile (S1–N2) is almost N–S along the East-African Rift. Both profiles intersect at the Afar Hotspot, at 42° of longitude. The 3D-model is calculated down to 400 km depth but its vertical resolution is poor below 300 km. The Afar hotspot signature is clearly observed over the whole depth range on both cross-sections, whereas a slow S_V-wave velocity anomaly is visible beneath the Gulf of Aden only down to 150 km depth.

On the W1-E2 cross-section, the amplitude of G parameter is the largest between longitudes 40°E to 55°E down to 150 km depth and the amplitude is weak below 200 km. The parameter δξ is positive ($V_{SH}>V_{SV}$ down to 150 km depth except below Afar and at 50°E. But it presents a succession of local minima close to Darfur and Tibesti hotspots, and maxima between Afar, Darfur, Tibesti and Hoggar hotspots in the depth range 50 to 150 km depth, separated approximately by 1000 km.

The distribution along the S1–N2 profile looks simpler than on the W1–E2 cross-section: there is a broad zone of low S_V -wave velocities (along the East-African Rift and the hotspot) located between positive amplitude zones below the Congo Craton at South and the Arabian shield at North, as expected from geology. The distribution of G parameter shows large amplitudes down to 200 km depth with minima below the Afar Hotspot and the Victoria hotspot. G displays very small values in a channel from Afar at 50 km and going deeper southward down to 140 km below Victoria hotspot and probably connected to west-African rift. On this cross-section, the radial anisotropy is almost everywhere strongly positive, except below Afar and the west-African rift. A low anisotropy channel of δξ (with respect to PREM) can be traced down from Afar, and perhaps connected to the minimum of δξ between 200–300 km depth at 0–3°N, 35°E. A striking feature is the large positive vertical anomaly of δξ below Afar between 150 km and 300 km, which might be associated with a strong deformation field.

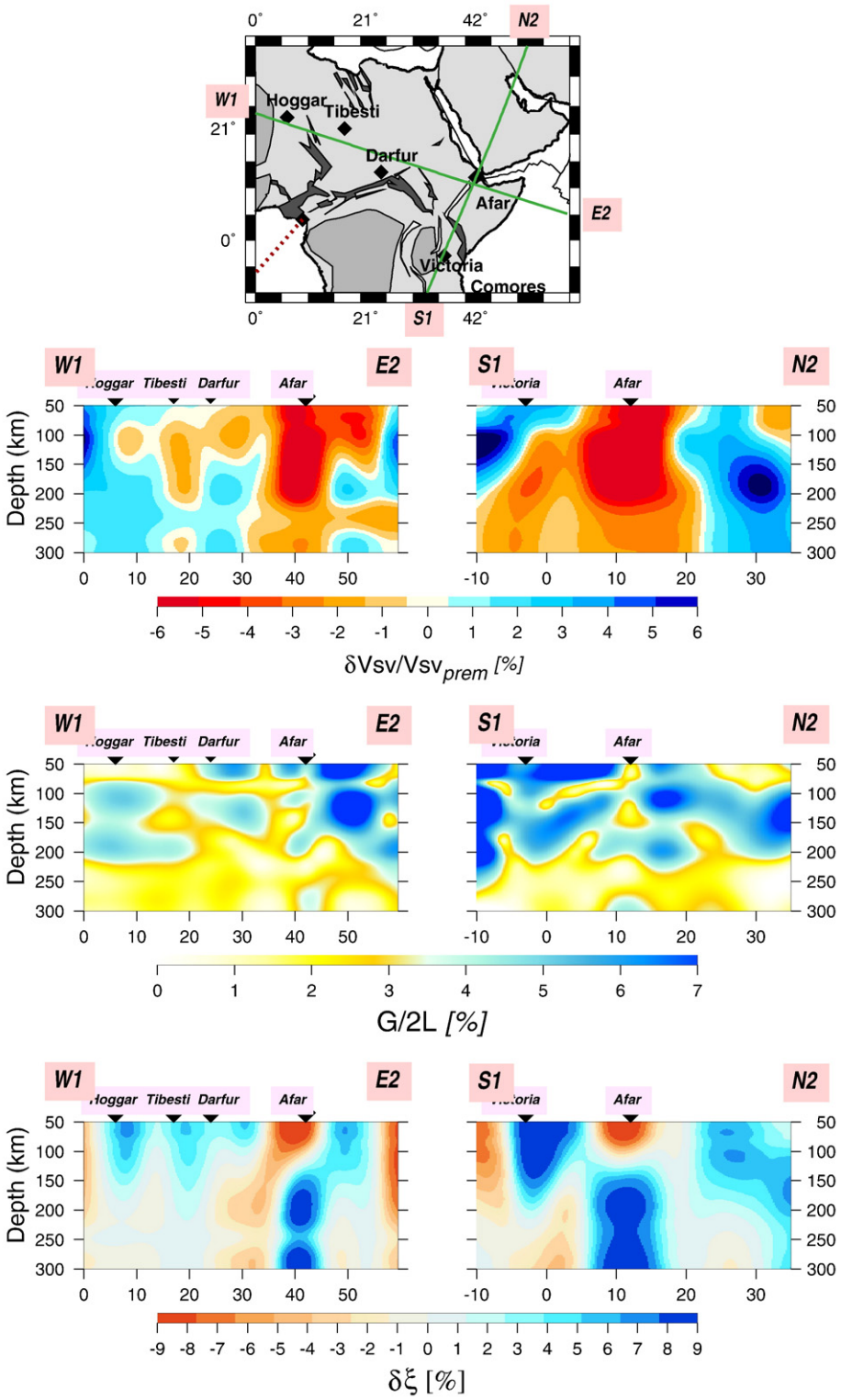

Fig. 8. Vertical cross-sections along great-circle path of profiles E–W (left) and N–S (right). (a) Shear-wave velocity distribution relative to PREM values. (b) Amplitude of parameter G (azimuthal anisotropy). (c) Values of parameter δξ (radial anisotropy). The sections are represented in function of depth and longitude for E–W cross-section and in function of depth and latitude for N–S cross-section. The hotspots are represented by diamonds on the map and black triangles on the vertical sections.

Therefore, the east-west structures in velocity and anisotropy in the top 200 km of the upper mantle show a dominant wavelength around 1000 km, whereas much longer wavelengths are visible in the south-north cross-section.

5.2. The Afar upwelling

Using only the fundamental mode of Rayleigh wave phase velocities for a regional study of Africa, the model of Ritsema and van Heijst (2000)

is consistent with the above-mentioned models but the resolution in the present study was improved by a factor 2 compared with this model. Moreover, their vertical cross-section of S_V -wave velocities drawn through the East-African Rift can be compared with profile S1–N2 on Fig. 8a. Both are very similar in the upper mantle, with a Tanzania craton extending down to 200 km–250 km and with a sharp transition to low-velocities beneath the East-African Rift in the northeast direction. In agreement with previous studies, a large and broad signature of low S_V-wave velocities is observed below the Afar Hotspot and the surrounding regions in the whole depth range. Although the use of fundamental mode does not give sufficient resolution at depth larger than 300 km, our fully anisotropic model through azimuthal and radial seismic anisotropies shows how the Afar upwelling can have influence even far from the hotspot on the asthenospheric flow. The time delay between the synthetic and the real signals recorded at the temporary station GDR (see Table 1 for location) in Ethiopia and mentioned in Section 3 is a direct evidence of this strong anomaly. The complex pattern of azimuthal anisotropy observed beneath the Horn of Africa might result from the presence of upwelling mantle material beneath the Afar Hotspot.

The cross section of profile W1-E2 on Fig. 8a shows a connection in the first 150 km between the slow anomalies of Afar and the Gulf of Aden. It probably means a feeding at the base of the lithosphere of the Gulf of Aden by the "Afar upwelling". This hypothesis is supported by a common geochemical signature of the plume to the Red Sea and Gulf of Aden (Marty et al., 1996). Nevertheless, the azimuthal anisotropy observed between 120 km and 250 km depth shows a W–WNW direction, west of Afar Hotspot. This could imply a west-northwest flow direction, at the base of the lithosphere. In spite of the weak lateral resolution of azimuthal anisotropy as retrieved from surface-wave studies, an important observation (Fig. 6b) is the strong change in anisotropy directions between Somalia–Arabia (almost south-north as found by Hansen et al., 2006) and west of Afar (east-west). If the LPO-flow interpretation is correct, the overall south-north asthenospheric flow seems to be deflected by the Afar upwelling. A robust result is that the south-north orientation of G is dominant in Africa north of 10°N below 120 km depth.

Anisotropy directions in the vicinity of ridges and hotspots can be examined in the light of the recent numerical calculations of Kaminski and Ribe (2002). Indeed, from theoretical calculations, they find that the perturbation of flow pattern around a plume is translated into anisotropic fast direction. The authors performed numerical calculations of the lattice preferred orientation (LPO) evolution in simple fluid dynamical models for ridge and for plume-ridge interaction. The results show how the LPO can be strongly perturbed in the proximity of the hotspot in a zone 5 times larger than the radius of the plume stem. Around Afar, the azimuthal anisotropy displays a very complex pattern (Fig. 6b) with rapid lateral variations, which is in agreement with a large plume head below the lithosphere becoming thinner at greater depths (>250 km). Kaminski and Ribe [2002] also define a dimensionless "grain orientation lag" parameter $\Pi(x)$ which is the ratio of the intrinsic LPO adjustment time scale to the time scale for changes in the finite strain direction. The fast axis of anisotropy is aligned with the flow direction only in those parts of the flow field where $\Pi \ll 1$, because in this case, the LPO has time to adjust to the local large finite strain. They show that close to the plume, Π is large, leading to a disrupted flow and a LPO poorly aligned with the flow direction. This shows that information on plume structure and its time evolution can be obtained not only from S_V-wave velocities but also from the distribution of azimuthal anisotropy.

Radial anisotropy is also perturbed by the presence of a mantle plume. In their model, Kaminski and Ribe (2002) observe a negative radial anisotropy ($V_{SV}>V_{SH}$) near ridge axis and a positive radial anisotropy ($V_{SH}>V_{SV}$) around the plume. This may explain the particularly strong anisotropic signature beneath and around Hawaii observed by Montagner and Tanimoto (1991), Ekström and Dziewonski (1998), Montagner (2002). Beneath Iceland, Gaherty (2001) finds negative values of radial anisotropy above ~100 km depth but positive values between ~120 and 300 km depth. He explains this anomalous anisotropy by the formation of a lithospheric fabric during hotspot-fueled buoyant upwelling at the ridge.

Our results on radial anisotropy enable us to get some new insight on the question of upper mantle flow beneath the Horn of Africa. Fig. 7 shows a zone around 100 km depth on the Aden Ridge with a positive ($V_{SV}<V_{SH}$) just east of Afar and then negative parameter $\delta\xi$ ($V_{SV}>V_{SH}$ when going east. This defines a subhorizontal flow close to Afar and an ascending material flow further east. It shows a very active upwelling associated with a very active tectonic area. This is in agreement with the strong azimuthal anisotropy at 100 km depth (Fig. 6b) which is induced by a strong strain field due to the regional extension. On the eastern side of Afar the flow can escape below the lithosphere towards the Indian Ocean and could have played a role in the opening of the Gulf of Aden, with the ridge propagating toward the Afar triple junction (Courtillot, 1982; Courtillot et al., 1999).

A similar observation is reported by Silveira and Stutzmann (2002) in the North Atlantic Ridge (between 20°N and 35°N), where the radial anisotropy is weak and the velocity anomaly is positive. This may be explained by a shallow structure and a passive feeding caused by the plate separation in the northern part of the ridge. Gung et al. (2003) also found a negative radial anisotropy along the East Pacific Rise down to 300 km, indicative of a significant component of vertical flow. On the other hand, following the common LPO interpretation, a clear signature in ξ with positive values, is found directly beneath the Afar Hotspot below 120 km, suggesting that the actual connection of the Afar Hotspot with deeper sources of upgoing material could be shifted laterally toward the south-west.

All these results show that seismic anisotropy is stratified beneath and around the Afar hotspot. At shallow depths (<100 km), fossil anisotropy and SPO (shape preferred orientation) anisotropy (Kendall et al., 2005) can be invoked, whereas at larger depths the LPO mechanism is dominant with strong changes of orientation, meaning at least 3 layers of anisotropy. The stratification of anisotropy emphasizes the difficulty to explain SKS data with simple models including one or two anisotropic layers.

5.3. Afar upwelling and Central Africa hotspots

A large number of hotspots exists in Central and East Africa (Afar, Hoggar, Tibesti, Darfur, Cameroon). They all present similarities in geological setting like volcanic swells, crustal thinning and petrology. Hadiouche et al. (1989) proposed based on a regional scale vectorial tomography study with a lateral resolution of 2000 km, a splitting of the plume in the first 250 km, suggesting a link between them. In the same way, Ebinger and Hayward (1996) addressed whether the so-called "Afar upwelling" could feed some hotspots of Central Africa. Ebinger and Sleep (1998) suggested that magmatism through most of continental Africa could be explained by a deep mantle plume with its first manifestation in Southern Ethiopia. However, Franz et al. (1999) do not see any connection from geochemical data, between the Darfur Hotspot on one side, and the Tibesti, the Cameroon Line and the volcanism of the Afar plume on the other side. For isotopic and chronological reasons, Ait Hamou (2000) also rejected the connection between Hoggar and Afar Hotspots. The isotopic signature of the Afar upwelling characterized by high $^3He/^4He$ ratios does not support such a connection since the other Cenozoic volcanic provinces (Darfur, Tibesti, Hoggar, Cameroon) have a different isotopic signature Montagner et al. (2007).

Looking at the W1-E2 profile in Fig. 8a, three low S_V-waves heterogeneities appear in the uppermost mantle at 5–10°E, 15–20°E and 25–30°E in addition to the big slow anomaly beneath Afar.

One low velocity spot finds its origin around 200 km depth and is centered on North of the Chad Lake close to the Tibesti hotspot. The other ones visible down to 150 km can be associated with the Hoggar hotspot and the Darfur hotspot. Around 30°E, a zone of fast velocities is extending from 100 km to large depth (Fig. 6a, depth = 100 km and Fig. 8a) and enables us to rule out a direct link between the Afar plume and the Central Africa hotspots in the asthenosphere. Because the results are robust above this depth, a possible connection could only occur at greater depths and probably by the southwestern part of the Afar region as suggested by the S_V-wave velocity perturbations at 200 km (Fig. 6a). But the helium data remain unexplained. These results are in agreement with the fast axis directions of the azimuthal anisotropy presented in Fig. 6b at 200 km, if we assume that this direction can be interpreted as the mantle flow direction (LPO mechanism). However, when considering the E–W cross-section, of parameters G and $\delta\xi$, small values of anisotropy at 15°E associated with low velocities down to 250 km suggest convective instabilities (or a secondary-scale convection cell) in the asthenosphere with questionable downwelling flows around 0°E along the west African craton and between 25°E and 30°E. The upwelling around 15°E (same longitude as Tibesti hotspot) is characterized by low velocities, small azimuthal anisotropy and negative radial ξ anisotropy down to 200 km.

The case of the Victoria hotspot seems more problematic. Low velocities are observed on the S1–N2 cross-section below the Victoria hotspot but they are not associated with small azimuthal and negative radial anisotropy (Fig. 8). However, small azimuthal and radial anisotropy is observed at −10°E at the boundary with the Tanzania craton. The Tanzania craton seems to be a shallower structure and displays fast velocity anomalies only down to 150–200 km depth. This fast velocity structure adjacent to the slow velocity structure of the rift might induce convective instabilites following the edge-driven convection process of King and Ritsema (2000). Below 200 km, it is difficult to say whether the slow velocities are related to the Victoria hotspot or not. As suggested by Weeraratne et al. (2003) they may be the signature of a plume, that we could see between 200 and 300 km depth below the Tanzania craton.

Therefore, the African continent shows two families of upwellings. Some upwellings beneath the Afar hotspot and possibly the Victoria hotspot, have a deep origin at least down to the transition zone. The signature of the Afar upwelling in the lower mantle is not obvious in the new model PRI-S05 (Montelli et al., 2006). Following the classification of Courtillot et al. (2003), and by using global tomography and fluid dynamics constraints, the Afar upwelling might be a primary plume, whose connection with the lower mantle might have already disappeared (Davaille et al., 2005). Others, such as the Central Africa hotspots (Darfur, Tibesti, Hoggar), have a superficial character, resulting from the interaction between lithosphere and asthenosphere. Their shallow signature and the distinction between a heterogeneous W–E structure and a relatively homogeneous and slow SW–NE profile following the East-African Rift (Fig. 8a) could suggest that the presence of the Central Africa hotspots is due to convective instabilities in the asthenosphere and/or are related to the edge-driven convection process (King and Ritsema, 2000) in a continental environment between cratons and more recent zones in north-central Africa. The typical continental breakup (see for example Courtillot et al., 1999) has been associated with the onset of hotspot and flood basalts. In that respect, the Afar upwelling was not completely successful for breaking up Africa along the East African rifts, but succeeded in the opening of the Red Sea and Gulf of Aden rifts. CASZ (Central Africa Shear Zone) might be an example of an aborted ridge, which presents lines of weaknesses and where the volcanic activity have been reactivated by the birth of the Afar hotspot through convective instabilities at the base of the lithosphere. The complex interaction between the Afar upwelling, the African lithosphere and asthenosphere has been revealed through the geographical distribution of seismic azimuthal and radial anisotropies.

Acknowledgments

This work has been supported by the INSU program Int'erieur de la Terre “Corne de l'Afrique” and benefited of 5 temporary stations from the INSU portable broad-band instrument pool. We thank the CFEE and the University of Addis Ababa, the Geophysical Observatory of Dhamar in Yemen, the CFY in Sanaa and the French embassies in Addis and Sanaa. Special thanks to Abdul-Hakim, Abdul-Jabbar Ahmed for their local support. Data were provided by the GEOSCOPE and IRIS teams and some of them were recorded by MEDNET and GEOFON networks and by the PASSCAL temporary stations.

Appendix 1. Shallow layer corrections

Surface waves are very sensitive to the crustal layers of Earth even at long period (Dziewonski 1971; Montagner and Jobert 1988). The crustal parts can thus affect and bias the determination of velocity anomalies at large depths, especially in the presence of a thick crust, e.g., Griot et al. (1998). However, Silveira et al. (1998) have shown that in oceanic regions, the crustal corrections do not change the location of heterogeneities. In the Afar region, where the Moho depth is not large, the corrections only have a small influence on the amplitude of anomalies. However, on a pure continental path crossing India, for example, the correction of the crustal effect increases the velocity by 0.057 km/s for a period of 100 s. Such a large amplitude means that it is necessary to correct for this effect. The corrections were applied before regionalization on individual paths (Montagner and Jobert, 1988). We computed for each path the phase velocity for the crustal part of a hybrid 3SMAC model (Nataf and Ricard, 1996). We subtracted the velocity of the PREM to isolate the crustal effect and removed it from the average phase velocity to obtain the corrected velocity. It must be noted that the crustal layers do not affect the results for anisotropy. Shallow layer corrections of phase velocities were also computed by using the CRUST2.0 model (upgrade of CRUST5.1 model of Mooney et al., 1998, but there is no significant difference in corrections compared with 3SMAC.

Appendix 2. Influence of higher modes on the Love waves phase velocities

The “roller coaster” method relies on a separation of time windows between the fundamental mode and the higher modes. Events with epicentral distances between 40° and 140° show Rayleigh wave fundamental mode well separated from the higher modes. However, for Love waves, the higher modes are propagating at nearly the same velocity as the fundamental mode. It is therefore more difficult to pick the different time windows. Nevertheless, since the higher modes are less energetic in comparison with the fundamental mode, Fig. A1 shows that they do not much affect the phase velocity measurement of the fundamental mode. We computed a perturbed model from PREM between 400 km and 700 km with S_H wave velocities increased to 4%. A synthetic seismogram is calculated up to the 6th mode-branch in this model and represents the “real” signal recorded for an event that occurred at 118 km depth and at an epicentral distance of 6481 km from the station. Another synthetic seismogram is computed for the same model but without higher modes. The phase velocity of the fundamental mode is inverted in both cases following the method described in Section 3 and the result is illustrated in Fig. A1 c. The influence of the higher modes on the fundamental mode phase velocity is less than 0.01 km/s (0.2%), which is not significant. The higher modes of an earthquake at 118 km are not sufficiently energetic

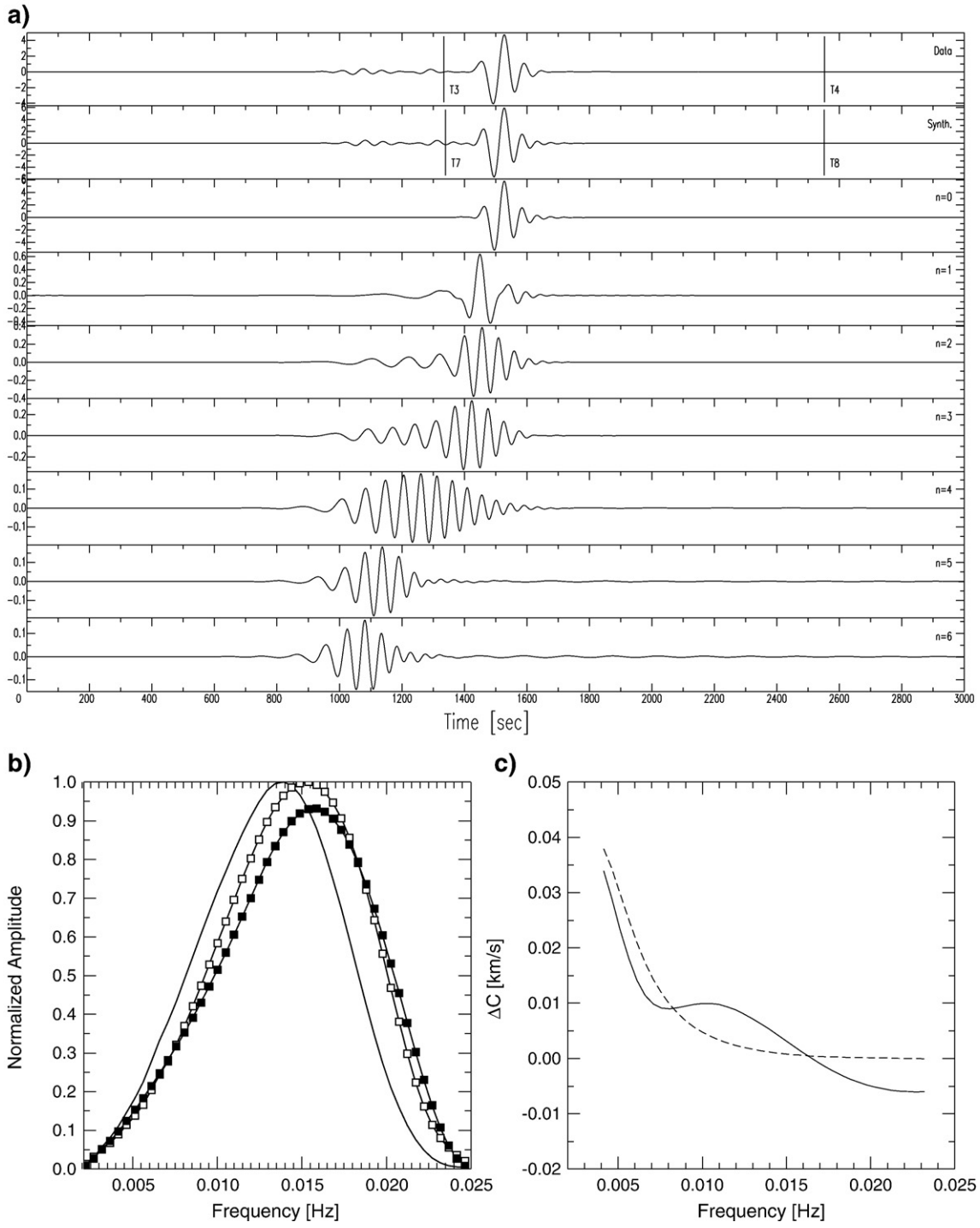

Fig. A1. (a) Synthetic seismogram computed in a perturbed model from PREM. The S_H-wave velocity is boosted by 4% between 400 km and 700 km. The corresponding synthetic seismogram and the contribution of 7 modes (fundamental mode $n=0$ to higher mode $n=6$) are also represented. The event occurred at 118 km depth and at 6481 km from the station. T3,T4,T7,T8 are defining the time windows of the fundamental mode for the "data" and its synthetic. (b) Spectra of real data (solid line), of the corresponding synthetic (white squares) and of the fundamental mode (black squares). (c) Results of phase velocities inversion for a data with higher modes (solid line) and a data only with fundamental mode (dotted line). The differences of phase velocities are represented relative to the PREM phase velocities.

to seriously bias the fundamental branch but for a deeper source the effect on the phase velocity could be larger.

References

Ait Hamou, F. (2000), Un exemple de "point chaud" intra-continental en contexte de plaque quasi-stationnaire: tude pétrologique et géochimique du djebel taharaq et évolution du volcanisme cénozoïque de l'ahaggar (sahara algérien), Ph.D. thesis, Univ. Montpellier II.

Anderson, D., 2000. The thermal state of the upper mantle; no role for mantle plumes. Geophys. Res. Lett. 27, 3623–3626.

Anderson, D., 2001. Topside tectonics. Science 293, 2016–2018.

Barberi, F., Ferrara, G., Santacroce, R., Varet, J., 1975. Structural Evolution of the Afar Triple Junction. Schweizerbart, Stuttgart.

Barruol, G., Ismail, W., 2001. Upper mantle anisotropy beneath the African IRIS and Geoscope stations. Geophys. J. Int. 146, 549–561.

Benoit, M., Nyblade, A., VanDecar, J., 2006. Upper mantle p-wave speed variations beneath ethiopia and the origin of the afar hotspot. Geology 34, 329–332. doi:10.1130/G22281.1.

Beucler, E., Stutzmann, E., Montagner, J., 2003. Measuring surface wave higher mode phase velocities, using a rollercoaster type algorithm. Geophys. J. Int. 155, 289–307.
Burke, K., Wilson, J., 1976. Hot spots on the earth's surface. Sci. Am. 235, 46–57.
Courtillot, V., 1982. Propagating rifts and continental breakup. Tectonics 1, 239–250.
Courtillot, V., Jaupart, C., Manighetti, I., Tapponnier, P., Besse, J., 1999. On causal links between flood basalts and continental breakup. Earth Planet. Sci. Lett. 166, 177–195.
Courtillot, V., Davaille, A., Besse, J., Stock, J., 2003. Three distinct types of hotspots in the Earth's mantle. Earth Planet. Sci. Lett. 205, 295–308.
Dahlen, F., Hung, S.H., Nolet, G., 2000. Fréchet kernels for finite-frequency traveltimes, i, theory. Geophys. J. Int. 141, 157–174.
Daly, M., Lawrence, S., Diemu-Tshiband, K., Matouana, B., 1992. Tectonic evolution of the Cuvette Centrale. Zaire, J. Geol. Soc. London 149, 539–546.
Davaille, A., 1999. Simultaneous generation of hotspots and superswells by convection in a heterogeneous planetary mantle. Nature 402, 756–760.
Davaille, A., Stutzmann, E., Silveira, G., Besse, J., Courtillot, V., 2005. Convective pattern in the indo-atlantic box. Earth Planet. Sci. Lett. 239, 233–252.
Debayle, E., Lévêque, J., 1997. Upper mantle heterogeneities in the Indian Ocean from waveform inversion. Geophys. Res. Lett. 24, 245–248.
Debayle, E., Kennett, B.L.N., 2000. Anisotropy in the Australasian upper mantle from Love and Rayleigh waveform inversion. Earth Planet. Sci. Lett. 184/1, 339–351.
Debayle, E., Lévêque, J.J., Cara, M., 2001. Seismic evidence for a deeply rooted low-velocity anomaly in the upper mantle beneath the northeastern Afro/Arabian continent. Earth Planet. Sci. Lett. 193, 423–436.
Debayle, E., Kennett, B., Priestley, K., 2005. Global azimuthal anisotropy and the unique plate-motion deformation of australia. Nature 433, 509–512.
Dziewonski, A.M., 1971. Upper mantle models from 'pure-path' dispersion data. J. Geophys. Res. 76, 2587–2601.
Ebinger, C., Hayward, 1996. Soft plates and hot spots: views from Afar. J. Geophys. Res. 101, 21,859–21,876.
Ebinger, C., Sleep, N.H., 1998. Cenozoic magmatism in Central and East Africa resulting from impact of one large plume. Nature 395, 788–791.
Ekström, G., Dziewonski, A.M., 1998. The unique anisotropy of the Pacific upper mantle. Nature 394, 168–172.
Ekström, G., Tromp, J., Larson, E., 1997. Measurements and global models of surface waves propagation. J. Geophys. Res. 102, 8137–8157.
Foulger, G., Pritchard, M., Julian, B., Evans, J., Allen, R., Nolet, G., Morgan, W., Bergsson, B., Erlendsson, P., Jakobsdottir, S., Ragnarsson, S., Stefansson, R., Vogfjörd, K., 2001. Seismic tomography shows that upwelling beneath Iceland is confined to the upper mantle. Geophys. J. Int. 146, 504–530.
Franz, F., Steiner, G., Volker, F., Pudlo, D., Hammerschmidt, K., 1999. Plume related alkaline magmatism in central Africa-the Meidob Hills (W Sudan). Chem. Geol. 157, 27–47.
Gaherty, J., 2001. Seismic evidence for hotspot-induced buoyant flow beneath the Reykjanes Ridge. Science 293, 1645–1648.
Gao, S., Davis, P., Liu, H., Slack, P., Rigor, A., Zorin, Y., Mordvinova, V., Kozhevnikov, V., Logatchev, N., 1997. SKS splitting beneath continental rift zones. J. Geophys. Res. 102, 22,781–22,797.
Grand, S., van der Hilst, R., Widiyantoro, S., 1997. Global seismic tomography: a snapshot of convection in the Earth. Geol. Soc. Am. Today 7 (No.4), 1–7.
Griot, D.A., Montagner, J.P., Tapponnier, P., 1998. Phase velocity structure from Rayleigh and Love waves in Tibet and its neighboring regions. J. Geophys. Res. 103, 21,215–21,232.
Gung, Y., Panning, M., Romanowicz, B., 2003. Global anisotropy and the thickness of continents. Nature 422, 707–711.
Hadiouche, O., Jobert, N., Montagner, J., 1989. Anisotropy of the African continent inferred from surface waves. Phys. Earth Planet. Inter. 58, 61–81.
Hansen, S., Schwartz, S., Al-Amri, A., Rodgers, A., 2006. Combined plate motion and density-driven flow in the asthenosphere beneath saudi arabia: evidence from shear-wave splitting and seismic anisotropy. Geology 34, 869–872.
Jestin, F., Huchon, P., 1992. Cinématique et déformation de la jonction triple mer Rouge-golfe d'Aden-Rift éthiopien depuis l'Oligocène. Bull. Soc. Geol. Fr. 163, 125–133.
Kaminski, E., Ribe, N., 2002. Time scales for the evolution of seismic anisotropy in mantle flow. Geochem. Geophys. Geosyst. 3. doi:10.1029/2001GC000.222.
Kendall, J.M., Stuart, G., Ebinger, C., Barstow, I., Keir, D., 2005. Magma-assisted rifting in ethiopia. Nature 433, 146–148.
King, S., Ritsema, J., 2000. African hot spot volcanism; small-scale convection in the upper mantle beneath cratons. Science 290, 1137–1140.
Knox, R., Nyblade, A., Langston, A., 1998. Upper mantle S velocities beneath Afar and western Saudi Arabia from Rayleigh wave dispersion. Geophys. Res. Lett. 25, 4233–4236.
Marty, B., Pik, R., Gezahagen, Y., 1996. He isotopic variations in Ethiopian plume lavas: nature of magmatic sources and limit on lower mantle convection. Earth Planet. Sci. Lett. 144, 223–237.
Mohr, P., 1983. Volcanotectonic aspects of Ethiopian evolution. Bull. Centre Rech. Explor.-Prod. ELF-Aquitaine 7, 157–189.
Montagner, J.P., 1986. Regional three-dimensional structures using long-period surface waves. Ann. Geophys. 4 (B), 283–294.
Montagner, J.P., 1994. Can seismology tell us anything about convection in the mantle? Rev. Geophys. 32 (2), 115–137.
Montagner, J.P., 2002. Upper mantle low anisotropy channels below the Pacific Plate. Earth Planet. Sci. Lett. 6320, 1–12.
Montagner, J.P., Jobert, N., 1981. Investigation of upper mantle structure under young regions of the Southeast Pacific using long-period Rayleigh waves. Phys. Earth Planet. Inter. 27, 206–222.
Montagner, J.P., Jobert, N., 1988. Vectorial tomography – II. Application to the Indian ocean. Geophys. J. 94, 309–344.
Montagner, J.P., Nataf, H., 1986. A simple method for inverting the azimuthal anisotropy of surface waves. J. Geophys. Res. 91, 511–520.
Montagner, J.P., Tanimoto, T., 1991. Global upper mantle tomography of seismic velocities and anisotropies. J. Geophys. Res. 96, 20,337–20,351.
Montagner, J.-P., Marty, B., Stutzmann, F., Sicilia, D., Cara, M., Pik, R., Lévêque, J., Roult, G., Debayle, E., Beucler, E., 2007. Mantle upwellings and convective instabilities revealed by seismic tomography and helium isotope geochemistry beneath eastern Africa. Geophys. Res. Lett. 34, L21303. doi:10.1029/2007GL031098.
Montelli, R., Nolet, G., Dahlen, F., Masters, G., Engdahl, E., Hung, S., 2004. Finite-frequency tomography reveals a variety of plumes in the Mantle. Science 303, 338–343.
Montelli, R., Nolet, G., Dahlen, F., Masters, G., 2006. Finite-frequency tomography reveals a variety of plumes in the mantle. Geochem. Geophys. Geosystem. 7 (Q11), 007. doi:10.1029/2006/2006GC001248.
Mooney, W., Laske, G., Masters, T., 1998. Crust 5.1: a global crustal model at 5deg×5deg. JGR 103, 727–747.
Morgan, W., 1971. Convection plumes in the lower mantle. Nature 230, 42–43.
Nataf, H.C., Ricard, Y., 1996. 3SMAC: an a priori tomographic model of the upper mantle based on geophysical modeling. Phys. Earth Planet. Inter. 95, 101–122.
Nicolas, A., Christensen, N.I., 1987. Formation of anisotropy in upper mantle peridotites: a review. In: Fuchs, C.F.E.K. (Ed.), Composition, Structure and Dynamics of the Lithosphere-Asthenosphere system. Geodyn. monogr. Ser., vol. 16. AGU, Washington, D.C, pp. 111–123.
Nishimura, C.E., Forsyth, D.W., 1989. The anisotropic structure of the upper mantle in the Pacific. Geophys. J. 96, 203–229.
Nyblade, A., 1994. The African superswell. Geophys. Res. Lett. 21, 765–768.
Nyblade, A., Knox, R., Gurrola, H., 2000. Mantle transition zone thickness beneath Afar: implications for the origin of the Afar hotspot. Geophys. J. Int. 142, 615–619.
Ritsema, J., van Heijst, H., 2000. New seismic model of the upper mantle beneath Africa. Geology 28, 63–66.
Ritsema, J., Ni, S., Helmberger, D., Crotwell, H., 1998. Evidence for strong shear velocity reductions and velocity gradients in the lower mantle beneath Africa. Geophys. Res. Lett. 25, 4245–4248.
Ritsema, J., van Heijst, H., Woodhouse, J., 1999. Complex shear wave velocity structure imaged beneath Africa and Iceland. Science 286, 1925–1928.
Sato, Y., Santo, T., 1969. World wide distribution of the group velocity of Rayleigh wave as determined by dispersion data. Bull. Earthq. Res. Inst. Univ. Tokyo 47, 31–41.
Sebai, A., Stutzmann, E., Montagner, J.P., Beucler, E., Sicilia, D., 2006. Hotspot and superswell beneath africa as inferred from surface wave anisotropic tomography. Phys. Earth Planet. Int. 155, 48–62.
Silveira, G., Stutzmann, E., 2002. Anisotropic tomography of the Atlantic ocean. Phys. Earth Planet. Inter. 132, 237–248.
Silveira, G., Stutzmann, E., Griot, D., Montagner, J.P., Mendes-Victor, L., 1998. Anisotropic tomography of the Atlantic ocean from Rayleigh surface waves. Phys. Earth Planet. Inter. 106/3–4, 259–275.
Smith, M., Dahlen, F., 1973. The azimuthal dependence of Love and Rayleigh wave propagation in a slightly anisotropic medium. J. Geophys. Res. 78, 3321–3333.
Stutzmann, E., Montagner, J.P., 1994. Tomography of the transition zone from the inversion of higher mode surface waves. Phys. Earth Planet. Inter. 86, 99–115.
Tarantola, A., Valette, B., 1982. Generalized nonlinear inverse problems solved using the least squares criterion. Rev. Geophys. Space Phys. 20, 219–232.
Weeraratne, D., Forsyth, D., Fisher, K., 2003. Evidence of an upper mantle plume beneath the Tanzanian craton from Rayleigh wave tomography. J. Geophys. Res. 108, 2427. doi:10.1029/2002JB002273.
Wilson, M., Guiraud, R., 1992. Magmatism and rifting in western and central Africa from late jurassic to recent times. Tectonophysics 213, 203–225.
Wolfe, C., Vernon III, F., Al-Amri, A., 1999. Shear waves splitting across Western Saudi Arabia. Geophys. Res. Lett. 26, 779–782.
Woodhouse, J., Girnius, T., 1982. Surface waves and free oscillations in a regionalized earth model. Geophys. J. R. Astron. Soc. 68, 653–673.